Journal of Magnetism and Magnetic Materials 475 (2019) 647–651

Contents lists available at ScienceDirect

Journal of Magnetism and Magnetic Materials

journal homepage: www.elsevier.com/locate/jmmm

Research articles

Multi-spectral Magnetic Particle Spectroscopy for the investigation of particle mixtures

T. Viereck, S. Draack, M. Schilling, F. Ludwig

Institute for Electrical Measurement Science and Fundamental Electrical Engineering, Technische Universität Braunschweig, Hans-Sommer-Straße 66, D-38106 Braunschweig, Germany

ARTICLE INFO

Keywords:
Magnetic Particle Spectroscopy
Magnetic nanoparticles
Quantification
Multi-spectral

ABSTRACT

Magnetic Particle Spectroscopy (MPS) records the non-linear response of magnetic nanoparticles (MNP) to large ac magnetic fields. It captures a harmonic spectrum for the characterization of MNP samples, especially in the context of Magnetic Particle Imaging (MPI). MPS is sensitive to minute variations in magnetization response, thus different particle types or batches are easily distinguished. Also, since the dynamic magnetization of the particles is driven by both the Néel and the Brownian relaxation mechanisms, the harmonic spectra in MPS scale with ambient parameters, such as temperature, viscosity or binding state of the particles. Previous studies mostly observed low-frequency harmonic ratios (e.g. $5f_0/3f_0$) to distinguish particles or to obtain ambient parameters. Here, we propose a multi-spectral analysis technique, using the full available spectrum, to decompose the collective response of different particles from an integral measurement on an MNP sample. This work focuses on the description of the multi-spectral method and its application to quantify binary and ternary mixtures of different particles.

1. Introduction

Magnetic Particle Spectroscopy (MPS) records the non-linear response of magnetic nanoparticles (MNP) to large ac magnetic fields [1]. It provides a measuring tool for the characterization of magnetic nanoparticles [2–4] and even allows for the estimation of ambient particle parameters, such as viscosity [5,6] or temperature [7–9]. It also facilitates a quantitative measure of particle concentrations (or iron content) in biological tissue [10–13]. Rauwerdink et al. demonstrated a simultaneous quantification of multiple MNPs by tracking low-frequency complex-valued harmonics [14], i.e. $3f_0$ and $5f_0$ of the excitation frequency f_0.

Here, we propose and experimentally verify a multi-spectral analysis technique, using the full available spectrum, to decompose the collective response of different particles from an integral measurement on an MNP sample. Incorporating more higher harmonics into the analysis improves the chance of separability and in general increases estimation accuracy. The method resembles the multi-spectral reconstruction technique used for multi-color Magnetic Particle Imaging [15], where different spectral responses can be resolved to constitute a functional imaging modality. Multi-color MPI has been successfully applied in interventional MPI [16] and for temperature estimation [17]. Our group developed a dual-frequency MPI scanner to monitor the particle mobility, i.e. viscosity or binding state, using a multi-spectral reconstruction approach [18,19].

Potential applications of the proposed method include the in vitro analysis of particles in a cell culture, where cell-ingested particles can be distinguished from those still in the culture medium (e.g. cell update study), or the discrimination of different particle types or particles in different states (i.e. temperature, viscosity/binding state, etc.). Multi-spectral MPS helps one to methodically investigate dependencies of the spectral response on the various particle parameters and to study the quantitativeness of the approach in a much simpler setting compared to MPI. Still the method and observed dependencies are - in general - translatable to an imaging experiment. In this contribution, we apply the multi-spectral method to analyze binary and ternary mixtures of different particles.

2. Spectral decomposition

The idea of multi-spectral analysis represents a measurement vector v as a linear combination of two (or more) reference measurements a_n, i.e. complex-valued harmonic spectra of a reference MNP sample. The coefficients α_n denote the contributions from the individual references a_n:

$$v = \sum_n \alpha_n a_n \tag{1a}$$

E-mail address: t.viereck@tu-bs.de (T. Viereck).

https://doi.org/10.1016/j.jmmm.2018.11.021
Received 23 June 2018; Received in revised form 22 October 2018; Accepted 4 November 2018
Available online 17 November 2018

$$= \alpha_1 \begin{pmatrix} a_{11} \\ \vdots \\ a_{m1} \end{pmatrix} + \ldots + \alpha_n \begin{pmatrix} a_{1n} \\ \vdots \\ a_{mn} \end{pmatrix} \tag{1b}$$

For multi-spectral MPS, a coefficient matrix A is assembled over the reference responses. Each column of A contains a full response spectrum with m harmonics of a reference sample (denoted in (1) by a_n and a_{mn}, respectively):

$$A = \begin{pmatrix} a_{11} & \ldots & a_{1n} \\ \vdots & \ddots & \vdots \\ a_{m1} & \cdots & a_{mn} \end{pmatrix} \tag{2}$$

Here, n is the number of references (typically $n = 2$ or $n = 3$) and m denotes the number of higher harmonic included in the measurement vector. For MPS purposes, the odd harmonics suffice (in contrast to MPI, where spatial encoding requires even harmonics as well). However, it might be beneficial to include even harmonic for e.g. dc field-dependent MPS measurements in order to improve the conditioning of the coefficient matrix. Generally, MPS data (above the limit of quantitation) provides an over-determined reference matrix A, since there are more harmonics in the measurement vector than number of reference points to attribute.

In order to obtain the α coefficients, we have to solve a simple $Ax = b$ linear equation. If A is the reference matrix and b the measurement vector, then x corresponds to α coefficients and yields the amount of contribution with respect to each reference. For that reason, the method is per se quantitative. For example, setting the iron content of a reference to 1 (normalization), then a sample with half or twice the concentration gives a coefficient of 0.5 or 2.0, respectively.

For solving the linear equation, a number of methods are available. Probably, the simplest choice is the so-called 'Truncated SVD' (TSVD) regularization method [20,21]. The TSVD method calculates a spectral decomposition by means of singular value decomposition (SVD):

$$A = U\Sigma V^T \approx U\Sigma_k V^T = A_k \tag{3}$$

The SVD of matrix A delivers left U and right V singular vector and a diagonal matrix Σ with singular values σ_i. For the purpose of regularization, only the k largest components (denoted by Σ_k) are considered in the solution x_{tsvd}:

$$x_{tsvd} = A_k^{-1} b \tag{4}$$

$$= V\Sigma_k^{-1} U^T b = \sum_{i=1}^{k} f_i \frac{u_i^T b}{\sigma_i} v_i \tag{5}$$

$$f_i := \begin{cases} 1 & i \leqslant k \\ 0 & i > k \end{cases} \tag{6}$$

TSVD performs an abrupt truncation of singular vectors, i.e. filter factors f_i are given by (6), which could lead to truncation artifact or oscillations.

The threshold parameter k, which is equivalent to a regularization parameter, is chosen minimal for our purpose, so that for two reference vectors we choose $k = 2$. Although, more advanced regularization schemes could be used, such as Tikhonov for which filter factors decay smoothly $f_i := \sigma_i^2/(\sigma_i^2 + \lambda^2)$ with regularization parameter λ there, the simple choice for k makes it a very straight forward method. Note that for TSVD k could be chosen larger, which would potentially even improve the decomposition. However, the reference basis would no longer be directly related to the calibration and therefore loose its meaning as physical quantity.

3. Methods and materials

3.1. Magnetic Particle Spectroscopy

In MPS, which is used as the measuring technique in this work, the magnetic nanoparticle sample is subjected to an alternating magnetic field in the lower kHz regime (e.g. 1 kHz) with a sufficiently large amplitude around 25 mT to partially saturate the particles ensemble. Inductive receiver coils detect the magnetization changes originating from the sample. The detection signal is pre-amplified and digitized for evaluation. MPS data reveals the dynamic non-linear magnetization behavior of the particles and is mostly represented either as a spectrum of higher harmonic components (via digital lock-in or FFT) or as a reconstructed dynamic magnetization curve.

Measurements were performed with a home-built Magnetic Particle Spectrometer that features a temperature-controlled sample holder and operates within a frequency range from 100 Hz to 25 kHz with differential receive coils, i.e. it is capable of recording the fundamental frequency [9, this issue]. The excitation frequency was set to $f_0 = 1$ kHz for all measurements. All sample measurements were carried out at room temperature (which can be considered constant for the duration of these measurements).

3.2. Nanoparticle samples

Samples were prepared as 10% diluted suspensions in microtiter vials of 150 µL volume each from stock solutions of commercially available tracers, i.e. SHP-25 from Ocean NanoTech (San Diego, California), perimag® from micromod Partikeltechnologie GmbH (Rostock, Germany) and FeraSpin™ XL from nanoPET Pharma GmbH (Berlin, Germany). Fig. 1 shows the magnitude harmonic spectra for all three particle systems.

The spectral responses of FeraSpin™ XL and perimag® (both multi-core) display qualitatively very similar behavior, whereas the harmonics for SHP-25 (single-core) decay much faster.

Structural properties of the individual tracers are summarized in Table 1.

All of the prepared samples (pure and mixtures) appeared stable by visual inspection and no signs of aggregation/agglomeration or even sedimentation were observed.

4. Experimental results

4.1. Binary mixtures

To validate the proposed decomposition method, we prepared a series of 3 binary mixtures of FeraSpin™ XL and perimag® in variable ratios plus the original tracers as reference samples. The FeraSpin™ content decreases from 100% for sample #1 linearly to 0% for sample #5 (perimag® content scales inversely). Fig. 2 shows the harmonic spectra obtained from MPS. The magnitude spectrum representation in Fig. 2(a) shows a typical MPS spectrum for multi core particles, but it does not provide any specifics of the binary mixture. However, the imaginary part (Fig. 2(b)) reveals two distinctive behaviors. While perimag (sample #5) shows a monotonous decay towards higher harmonic indices, FeraSpin XL (sample #1) features a maximum in the

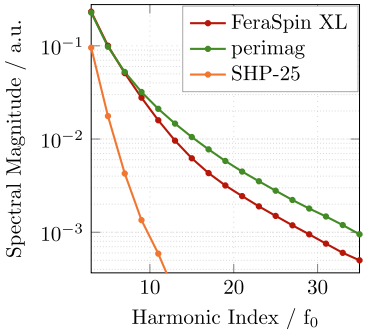

Fig. 1. Magnitude harmonic spectra of all three particles used in this study.

Table 1
Structural properties (effective core diameter $d_{c,eff}$ and hydrodynamic diameter d_h) of the tracer particles.

	SHP-25	Perimag	FeraSpin XL
$d_{c,eff}$	25 nm	19 nm	23 nm
d_h	35–40 nm	120–130 nm	50–60 nm
type	single core	multi core	multi core

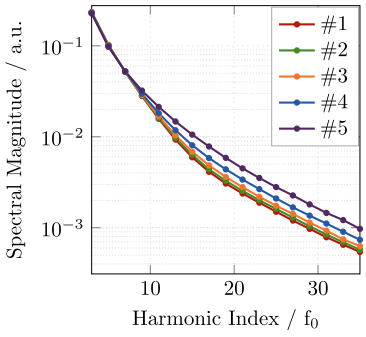

(a) Magnitude of harmonic spectrum

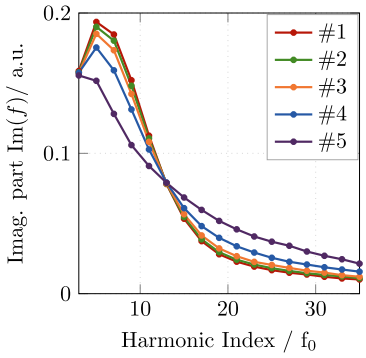

(b) Imaginary part of spectrum ($3f_0$ normalized)

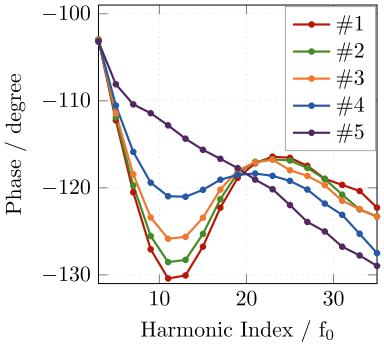

(c) Phase of harmonic spectrum

Fig. 2. Different representations of harmonic spectra on binary mixtures measured at 1 kHz. Sample #1 denotes pure FeraSpin, #5 pure perimag, and the remaining samples are linear mixing ratios in between.

imaginary part between $3f_0$ and $5f_0$. All mixtures (samples #2–#4) are - by visual inspection - superpositions of the two pure tracers. The observation in the imaginary part is supplemented by the phase behavior of the samples (Fig. 2(c)). Again, FeraSpin XL (sample #1) shows a pronounced phase behavior, whereas perimag exhibits an almost linear phase. Fig. 2(b) and (c) motivate the need for complex-valued evaluation of the MPS data in order to discriminate particle mixtures, as it was also observed in [14].

Table 2
Mixing ratios of binary mixture: for each sample, the expected percentage (from pipetting preparation) is denoted by 'actual', the reconstructed estimate by 'est.(imate)'.

	FeraSpin XL		Perimag		
	Actual	Est.	Actual	Est.	sum_{est}
#1	1.00	1.00	0.00	0.000	1.00
#2	0.75	0.741	0.25	0.277	1.02
#3	0.50	0.483	0.50	0.529	1.01
#4	0.25	0.226	0.75	0.807	1.03
#5	0.00	0.000	1.00	1.000	1.00

The quantitative composition of the binary particle mixtures estimated via the multi-spectral technique is listed in Table 2. The reference samples (samples #1 and #5) are reconstructed without any deviation. This is expected behavior and shows that we indeed obtain a decomposition onto the reference basis.

The relative estimation error of the reconstructed ratios (in reference to expected ratio, set value) is around 10% (Note: the set value includes an unknown pipetting error from sample preparation). Though, the iron content (= sum of both contributions, sum_{actual} in Table 2) is estimated within an 3.3% error margin. For that reason, the larger estimation error for the ratios can arguably be attributed to the decomposition method itself rather than to the sample preparation. A graphical representation of the expected and estimated mixing ratios is given in Fig. 3.

4.2. Ternary mixtures

We also prepared ternary mixtures of nanoPET FeraSpin™ XL, micromod perimag® and Ocean NanoTech SHP-25 (see Fig. 4). The series consists of 13 samples total. Three samples are the pure tracers for reference. Three more samples provide all possible combinations of binary mixtures with only two tracers each. And 7 samples are ternary mixtures with variable ratios of all three tracers.

Fig. 4(a) depicts the estimated ratios (blue dots) in comparison with the actual mixing ratios (red dots) of the MNP mixtures. Each axis of the 3-dimensional cube represents one tracer. By visual inspection, blue and red dots deviate more around the cube center (ternary mixtures), while at the edges and corners a good agreement is observed. Numerically, the estimation errors for binary mixtures are comparable to the previous section, while ternary mixtures are reconstructed with a higher error margin of up to 18%. In Fig. 4(b) a quantitative analysis of the estimated mixing ratios is provided. We plot the estimated content as a function of the actual content, separately for each tracer. As can be seen, a high level of agreement is achieved. SHP-25 (single core tracer) shows the smallest quantification error, while FeraSpin and perimag (both multi core tracers) exhibit a negative and positive offset,

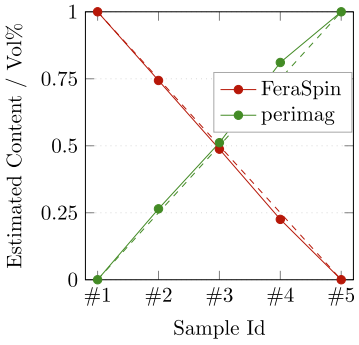

Fig. 3. Reconstruction of sample content in binary mixtures: Data points and solid lines denote estimated ratios, dashed lines show the actual ratios.

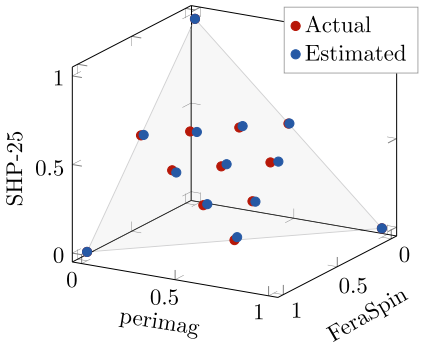

(a) Estimated ratios of ternary mixtures

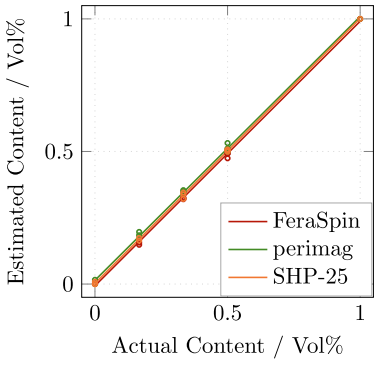

(b) Quantitative analysis of mixture ratios

Fig. 4. Reconstruction of sample content in ternary mixtures of FeraSpin™ XL, perimag® and SHP-25. Qualitative comparison of estimated and actual content (a) and quantitative analysis of mixture composition (b).

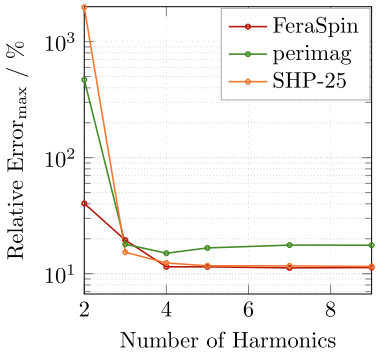

Fig. 5. Relative estimation error (maximum across all samples) as a function of the number of higher harmonics used in the decomposition.

respectively. Still, the overall estimation accuracy is found to be excellent and no mixing artifacts are found (i.e. no interaction of the different particles).

The estimation accuracy represented by the largest relative error (across all measured samples) as a function of the number of higher harmonics included in the decomposition schema is plotted in Fig. 5. The graph gives an upper error bound for the decomposition method. The average estimation error is usually much smaller. The estimation error is very large if an under-determined system is constructed, i.e. if the number of considered harmonics is less than the number of references. In fact, the error only drops into the 10% range once both numbers agree. Including more harmonics, even those with poor signal-to-noise ratio, does not have any negative impact on the decomposition quality, i.e. the regularization produces stable results (tested up to 50 harmonics). Therefore, the choice of harmonics number is not critical. As a general observation (not all data is shown here), less characteristic spectra accumulate larger estimation errors. For samples with strong harmonic decay, such as SHP-25 in this study, the complex spectral amplitude can be rescaled logarithmically, to amplify the contribution of high frequency components. For the estimation error to stay within certain bounds, a threshold number of harmonics can always be determined from the error graph (cp. Fig. 5). The threshold greatly varies for different particle systems and depending on the structure of the spectral responses. For example, discrimination of viscosities with FeraSpin XL typically requires at least 7f through 11f to be included, since significant differences are observed in and above that range and the estimation error then gradually decreases with additional harmonics.

5. Discussion and outlook

In this contribution, we proposed a simple regularized decomposition method, the (well-known) truncated SVD algorithm, to achieve a simultaneous quantification of up to three different tracers from a single integral MPS measurement. In contrast to previous reports, the method uses the full harmonic spectrum as a basis for decomposition. This way we take advantage of the signal structure at higher harmonic indices, which suggest that especially for multi core particle, where we typically observe a response with two distinct trends, an improvement in estimation accuracy can be expected. Here, for all estimates the algorithm considered 9 odd harmonic components (up to $19f_0$). We found that a reasonable distinction of three MNP types is possible from 3–4 harmonics onwards. However, the estimation accuracy benefits from additional information in the higher harmonics, as long as a minimal SNR margin is maintained. A high degree of redundancy in the spectral MNP response for ternary mixture suggests that even more tracer types (or properties) could be explored by multi-spectral MPS. Considering the wideband response, we can translate our findings to MPI. However, only in MPS a highly over-determined coefficient matrix is available, which makes multi-spectral MPS a valuable tool in diagnostics and tracer characterization.

A further improvement could potentially be achieved via parametric MPS measurements, i.e. as a function of frequency, field-amplitude, and dc amplitude.

Future research will look at the orthogonality of different tracer responses and tracer parameters and will especially explore viscosity and temperature as the two most important parameters.

Acknowledgements

Financial support by the German Research Foundation DFG via SPP1681 (VI892/1–1) and Niedersächsisches Vorab through Quantum- and Nano-Metrology (QUANOMET) initiative within the project NP-2 are acknowledged.

References

[1] S. Biederer, T. Knopp, T.F. Sattel, K. Ldtke-Buzug, B. Gleich, J. Weizenecker, J. Borgert, T.M. Buzug, Magnetization response spectroscopy of superparamagnetic nanoparticles for magnetic particle imaging, J. Phys. D: Appl. Phys. 42 (20) (2009) 205007, https://doi.org/10.1088/0022-3727/42/20/205007.

[2] F. Ludwig, H. Remmer, C. Kuhlmann, T. Wawrzik, H. Arami, R. Ferguson, K. Krishnan, Self-consistent magnetic properties of magnetite tracers optimized for magnetic particle imaging measured by ac susceptometry, magnetorelaxometry and magnetic particle spectroscopy, J. Magn. Magn. Mater. 360 (2014) 169–173, https://doi.org/10.1016/j.jmmm.2014.02.020.

[3] F. Ludwig, C. Kuhlmann, T. Wawrzik, J. Dieckhoff, A. Lak, A. Kandhar, R. Ferguson, S. Kemp, K. Krishnan, Dynamic magnetic properties of optimized magnetic nanoparticles for magnetic particle imaging, IEEE Trans. Magn. 50 (11) (2014), https://doi.org/10.1109/TMAG.2014.2329504.

[4] C. Kuhlmann, A.P. Khandhar, R.M. Ferguson, S. Kemp, T. Wawrzik, M. Schilling, K.M. Krishnan, F. Ludwig, Drive-field frequency dependent MPI performance of single-core magnetite nanoparticle tracers, IEEE Trans. Magn. 51 (2) (2015) 1–4, https://doi.org/10.1109/tmag.2014.2329772.

[5] A.M. Rauwerdink, J.B. Weaver, Measurement of molecular binding using the Brownian motion of magnetic nanoparticle probes, Appl. Phys. Lett. 96 (3) (2010)

033702, https://doi.org/10.1063/1.3291063.
[6] A.M. Rauwerdink, J.B. Weaver, Viscous effects on nanoparticle magnetization harmonics, J. Magn. Magn. Mater. 322 (6) (2010) 609–613, https://doi.org/10.1016/j.jmmm.2009.10.024.
[7] J.B. Weaver, A.M. Rauwerdink, E.W. Hansen, Magnetic nanoparticle temperature estimation, Med. Phys. 36 (5) (2009) 1822–1829, https://doi.org/10.1118/1.3106342.
[8] I.M. Perreard, D.B. Reeves, X. Zhang, E. Kuehlert, E.R. Forauer, J.B. Weaver, Temperature of the magnetic nanoparticle microenvironment: estimation from relaxation times, Phys. Med. Biol. 59 (5) (2014) 1109–1119, https://doi.org/10.1088/0031-9155/59/5/1109.
[9] S. Draack, T. Viereck, C. Kuhlmann, M. Schilling, F. Ludwig, Temperature-dependent MPS measurements, Int. J. Magn. Particle Imaging, Vol. 3, No. 1, Article ID 1703018 doi: https://doi.org/10.18416/ijmpi.2017.1703018.
[10] A. Lindemann, B.M. Fraederich, R. Pries, B. Wollenberg, K. Ldtke-Buzug, K. Graefe, Biological impact of superparamagnetic iron oxide nanoparticles for magnetic particle imaging of head and neck cancer cells, Int. J. Nanomed. 5025 (2014), https://doi.org/10.2147/ijn.s63873.
[11] C. Grfe, I. Slabu, F. Wiekhorst, C. Bergemann, F. von Eggeling, A. Hochhaus, L. Trahms, J.H. Clement, Magnetic particle spectroscopy allows precise quantification of nanoparticles after passage through human brain microvascular endothelial cells, Phys. Med. Biol. 61 (11) (2016) 3986–4000, https://doi.org/10.1088/0031-9155/61/11/3986.
[12] W.C. Poller, N. Lwa, F. Wiekhorst, M. Taupitz, S. Wagner, K. Mller, G. Baumann, V. Stangl, L. Trahms, A. Ludwig, Magnetic particle spectroscopy reveals dynamic changes in the magnetic behavior of very small superparamagnetic iron oxide nanoparticles during cellular uptake and enables determination of cell-labeling efficacy, J. Biomed. Nanotechnol. 12 (2) (2016) 337–346, https://doi.org/10.1166/jbn.2016.2204.
[13] N. Lwa, M. Seidel, P. Radon, F. Wiekhorst, Magnetic nanoparticles in different biological environments analyzed by magnetic particle spectroscopy, J. Magn. Magn. Mater. 427 (2017) 133–138, https://doi.org/10.1016/j.jmmm.2016.10.096.
[14] A.M. Rauwerdink, A.J. Giustini, J.B. Weaver, Simultaneous quantification of multiple magnetic nanoparticles, Nanotechnology 21 (45) (2010) 455101, https://doi.org/10.1088/0957-4484/21/45/455101.
[15] J. Rahmer, A. Halkola, B. Gleich, I. Schmale, J. Borgert, First experimental evidence of the feasibility of multi-color magnetic particle imaging, Phys. Med. Biol. 60 (5) (2015) 1775–1791, https://doi.org/10.1088/0031-9155/60/5/1775.
[16] J. Haegele, S. Vaalma, N. Panagiotopoulos, J. Barkhausen, F.M. Vogt, J. Borgert, J. Rahmer, Multi-color magnetic particle imaging for cardiovascular interventions, Phys. Med. Biol. 61 (16) (2016) N415–N426, https://doi.org/10.1088/0031-9155/61/16/n415.
[17] C. Stehning, B. Gleich, J. Rahmer, Simultaneous magnetic particle imaging (MPI) and temperature mapping using multi-color MPI, International Journal on Magnetic Particle Imaging, Vol. 2, No. 2, Article ID 1612001 doi: https://doi.org/10.18416/ijmpi.2016.1612001.
[18] M. Schilling, F. Ludwig, C. Kuhlmann, T. Wawrzik, Magnetic particle imaging scanner with 10-kHz drive-field frequency, Biomed. Tech. 58 (6) (2013) 557–563, https://doi.org/10.1515/bmt-2013-0014.
[19] T. Viereck, C. Kuhlmann, S. Draack, M. Schilling, F. Ludwig, Dual-frequency magnetic particle imaging of the Brownian particle contribution, J. Magn. Magn. Mater. 427 (2017) 156–161, https://doi.org/10.1016/j.jmmm.2016.11.003.
[20] P.C. Hansen, The truncated SVD as a method for regularization, BIT 27 (4) (1987) 534–553, https://doi.org/10.1007/bf01937276.
[21] R.D. Fierro, G.H. Golub, P.C. Hansen, D.P.O. Leary, Regularization by truncated total least squares, SIAM J. Sci. Comput. 18 (4) (1997) 1223–1241, https://doi.org/10.1137/s1064827594263837.